

Automatic Anatomy Recognition on CT Images with Pathology

Lidong Huang^{a,b}, Jayaram K. Udupa^b, Yubing Tong^b, Dewey Odhner^b, Drew A. Torigian^b
^aCollege of Information and Communication Engineering, Beihang University, Beijing 100083, China; ^bMedical Image Processing Group, Department of Radiology, University of Pennsylvania, Philadelphia, PA;

ABSTRACT

Body-wide anatomy recognition on CT images with pathology becomes crucial for quantifying body-wide disease burden. This, however, is a challenging problem because various diseases result in various abnormalities of objects such as shape and intensity patterns. We previously developed an automatic anatomy recognition (AAR) system [1] whose applicability was demonstrated on near normal diagnostic CT images in different body regions on 35 organs. The aim of this paper is to investigate strategies for adapting the previous AAR system to diagnostic CT images of patients with various pathologies as a first step toward automated body-wide disease quantification. The AAR approach consists of three main steps – model building, object recognition, and object delineation. In this paper, within the broader AAR framework, we describe a new strategy for object recognition to handle abnormal images. In the model building stage an optimal threshold interval is learned from near-normal training images for each object. This threshold is optimally tuned to the pathological manifestation of the object in the test image. Recognition is performed following a hierarchical representation of the objects. Experimental results for the abdominal body region based on 50 near-normal images used for model building and 20 abnormal images used for object recognition show that object localization accuracy within 2 voxels for liver and spleen and 3 voxels for kidney can be achieved with the new strategy.

Keywords: Image segmentation, diagnostic CT images, fuzzy models, object recognition, anatomy recognition

1. INTRODUCTION

Automatic disease quantification based on Computed Tomography (CT) images is useful for clinical research and the practice of evidence-based medicine. Body-wide anatomy recognition is an important first step for accurately and automatically quantifying diseases via CT images [2, 3]. However, the recognition or localization of objects with pathology on CT images has remained a challenge due to the presence of deviations from normalcy in object shape and intensity patterns.

Many image segmentation methods have been investigated and applied to CT images, but mostly for segmenting organs in normal CT images. These include thresholding, region growing, clustering, deformable model driven techniques, and graph based approaches [4-7]. A few previous works studied anatomy recognition on CT images with pathology, but mostly by focusing on one specific object without considering multiple objects in the whole-body [8-13]. The generalizability of these methods to a different organ/object or body region is not clear, and to our knowledge none have demonstrated this on diagnostic CT images with pathology. Therefore, the development of a robust object localization/recognition method that works on diagnostic CT images with pathology body-wide would constitute an advancement of the state-of-the-art in diagnostic CT quantitative image analysis.

Motivated by body-wide applications and generalizability of methods, and particularly body-wide automatic disease quantification, we have recently developed a general automatic anatomy recognition (AAR) methodology and demonstrated its operability in three different body regions on over 35 objects in contrast-enhanced diagnostic CT and MR images [1]. The AAR approach consists of the following three main steps: model building, object recognition, and object delineation. A hierarchical fuzzy anatomy model of a body region with all its major objects or a subset of them is built in the model building step. Recognition is a high-level process of determining the whereabouts of the object in the image. Delineation is a low-level process of determining the precise spatial extent of the object in the image. The AAR approach was demonstrated and validated on near normal images from three different body regions – neck, thorax, and abdomen, involving over 35 organs for both the recognition and delineation tasks. We considered it important to

understand the behavior of the general AAR methodology on images with no or minor abnormalities and hence did not study the behavior of the methodology on abnormal images.

The aim of this paper is to investigate modifications needed for adapting the previous AAR system to diagnostic CT images of patients with various pathologies as a first step toward automated body-wide disease quantification. In the next section we describe these adaptations while keeping the generality of the original approach. Subsequently, we will describe our evaluations, experimental results, and conclusions.

2. MODIFIED AAR APPROACH FOR IMAGES WITH PATHOLOGY

It is demonstrated in [1] that good recognition can guarantee good delineation accuracy. In this paper, we focus only on the recognition step and propose modifications to the recognition process in order to achieve good recognition performance on diagnostic CT images containing pathology. Modifications are done to both steps: constructing fuzzy models and recognizing objects. We will highlight mainly the differences from the previous AAR approach; please refer to [1] for details on the original methodology.

2.1 Constructing fuzzy models

In [1], a population model for a given subject group is built for an entire body region. This model, called Fuzzy Anatomy Model $FAM(B, G)$ for a body region B of subject group G is described by a quintuple: $FAM(B, G) = (H, M, \rho, \lambda, \eta)$ [1]. The meaning of the elements of this body region model are described below.

In this paper, for demonstration of the ideas, we will focus on the abdominal body region and the following six objects in the abdominal body region: Outer boundary of abdominal skin (ASkn), Liver (Lvr), Right kidney (RKd), Left kidney (LKd), both kidneys together as a composite object (Kd), and Spleen (Spln). H is a hierarchy of objects in B . That is, the objects are considered in a certain hierarchical structure and not flatly just as a collection. The AAR approach follows strict definitions of body regions and objects [1] and in this paper we will follow the regimen described in [1]. Figure 1 shows the hierarchy used in this study for the six objects.

$M = \{FM_\ell: 1 \leq \ell \leq L\}$ is a set of fuzzy models, one fuzzy model per object. FM_ℓ represents the fuzzy model of object O_ℓ . The fuzzy model FM_ℓ encodes the variations in the object's form over G and is independent of image intensity and modality. FM_ℓ is constructed from training binary images for the object. Briefly, this process consists of estimating the mean shape length and geometric center of the object over G , repositioning all samples of the object to this mean position, and rescaling them to mean shape length. Subsequently a distance transform is applied to each resulting sample to propagate the shape form inward and outward from its boundary, the distance values are then averaged, and the average distance is transformed to a fuzzy object membership value.

$\rho = \{\rho_\ell: 1 \leq \ell \leq L\}$ where ρ_ℓ denotes the parent-to-offspring relationship in H over G of offspring object O_ℓ with respect to its unique parent. From the repositioned and resized samples, the parent-to-offspring relationship ρ_ℓ of O_ℓ in the hierarchy is estimated over G . $\lambda = \{\lambda_\ell: 1 \leq \ell \leq L\}$ and λ_ℓ is the scale factor range indicating the size variation of object O_ℓ over G . This parameter is also estimated over G from the repositioned and resized samples. η represents a set of measurements pertaining to the objects in B .

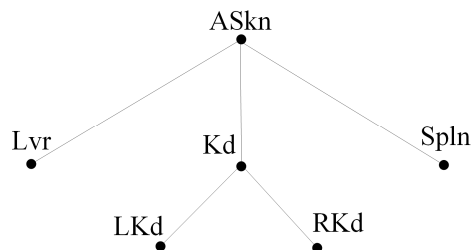


Figure 1. Object hierarchy used in this study. ASkn: Outer boundary of abdominal skin; Lvr: Liver; Kd: Kidneys; RKd: Right kidney; Lkd: Left kidney; Spln: Spleen.

2.2 Recognizing objects

The objects are recognized in the hierarchical order. In the earlier AAR approach, the optimal pose for O_ℓ in a test image I is found in two steps. In the first step, called *one-shot* recognition, the pose of O_ℓ is determined directly from the pose of its parent, once the recognition of the parent object in I is completed, and the known parent-to-offspring relationship ρ_ℓ stored in the fuzzy anatomy model of B . In the second step, this pose is refined by finding the pose with which we can minimize the sum of the volume of false positive and false negative regions between the transformed fuzzy model $FM^p(O_\ell)$ and the binary image J resulting from thresholding I using a threshold interval Th_ℓ associated with O_ℓ [1].

$$p^* \in \arg \min_p (|FM^p(O_\ell) - J| + |J - FM^p(O_\ell)|). \quad (1)$$

Image subtraction here is done in the sense of fuzzy logic. $|x|$ denotes the fuzzy cardinality of x . The search space to find p^* is limited to a region around the initial pose. The search region is determined from knowledge of ρ_ℓ and its variation and the scale factor range λ_ℓ . An optimal threshold interval Th_ℓ is determined for O_ℓ by rehearsing a recognition trial on the training images that yields the best recognition accuracy. See [1] for details.

In the new AAR process, the second step of optimal search is modified. The modification is based on the premise that, if we randomly sample a spherical ball region b_ℓ in I within the region defined by the current fuzzy model, that sample is likely not to contain pathology. The ball radius R_ℓ is set proportional to the size of O_ℓ ; $R_\ell = k \times size(O_\ell)$. The ball center is chosen to be within the model by one of several methods – at the geometric center of the model, at a point that is most medial, etc. For non-blob like objects with concavities, the latter criterion may fail. However for the objects considered in this paper, this method works. Having chosen the ball, the AAR pre-learned threshold Th_ℓ is refined to find a new optimal threshold T_ℓ that would maximize the number of voxels $N_\ell(t, b_\ell, I)$ in the ball that satisfy this threshold.

$$T_\ell \in \arg \max_{Th_\ell - \delta \leq t \leq Th_\ell + \delta} N_\ell(t, b_\ell, I). \quad (2)$$

The coverage $N_\ell(t, b_\ell, I)$ is a measure of segmentation of near normal object tissue within the ball. Greater coverage implies better ability to localize O_ℓ . In our experiments, the two parameters k and δ are set to 0.3 and 50 Hounsfield Units, respectively. The refined threshold T_ℓ is subsequently used in an AAR recognition process as described in (1).

3. EXPERIMENTAL RESULTS

3.1 Data sets and model building

This retrospective study was conducted following approval from the Institutional Review Board at the Hospital of the University of Pennsylvania along with a Health Insurance Portability and Accountability Act waiver. Two data sets are employed in our experiments. DS1: contrast-enhanced abdominal diagnostic CT images of 50 male subjects with age in the range 50-60 years who were radiologically normal with exception of minimal incidental focal abnormalities; this image data set was one of the data sets used in [1]. DS2: contrast-enhanced abdominal diagnostic CT images of 20 male and female cancer patients (not necessarily in the above age range) with various pathologies involving one or more solid organs depicted in Figure 1. The image data sets were selected from our hospital patient image database. The voxel sizes for the two data sets are approximately 0.9 mm x 0.9 mm x 5 mm, which constitute typical clinical resolutions commonly employed in the abdomen.

All objects considered in this paper were manually segmented using user-driven interactive tools such as live wire and iterative live wire which provided the reference segmentations. All samples in data set DS1 are used for model building and DS2 is used for testing the new AAR approach.

3.2 Recognition on CT images with pathology

Figure 2 displays sample recognition results for the new AAR approach on images from DS2. The figures display cross sections of the fuzzy models at recognition overlaid on the test image slices. The image slices are also displayed separately to visualize the underlying pathology.

We use location error and size error to evaluate recognition results quantitatively. Location error denotes the distance between the centers of ground truth objects and the fuzzy model at optimal recognition. Scale error denotes the ratio of the estimated object size to true object size. Ideally the location or position error should be zero and size error should be 1. Table 1 lists the mean and standard deviation of location error and size error over all images in data set DS2 for the objects shown in Figure 1. As we can see from Table1, the average position errors are within 2 voxels for liver and spleen and 3 voxels for kidney, and average size errors are all close to 1. Generally speaking, the modified AAR shows consistent and good recognition performance on CT images with pathology for the objects considered in this paper. This is crucial for quantifying body-wide disease burden.

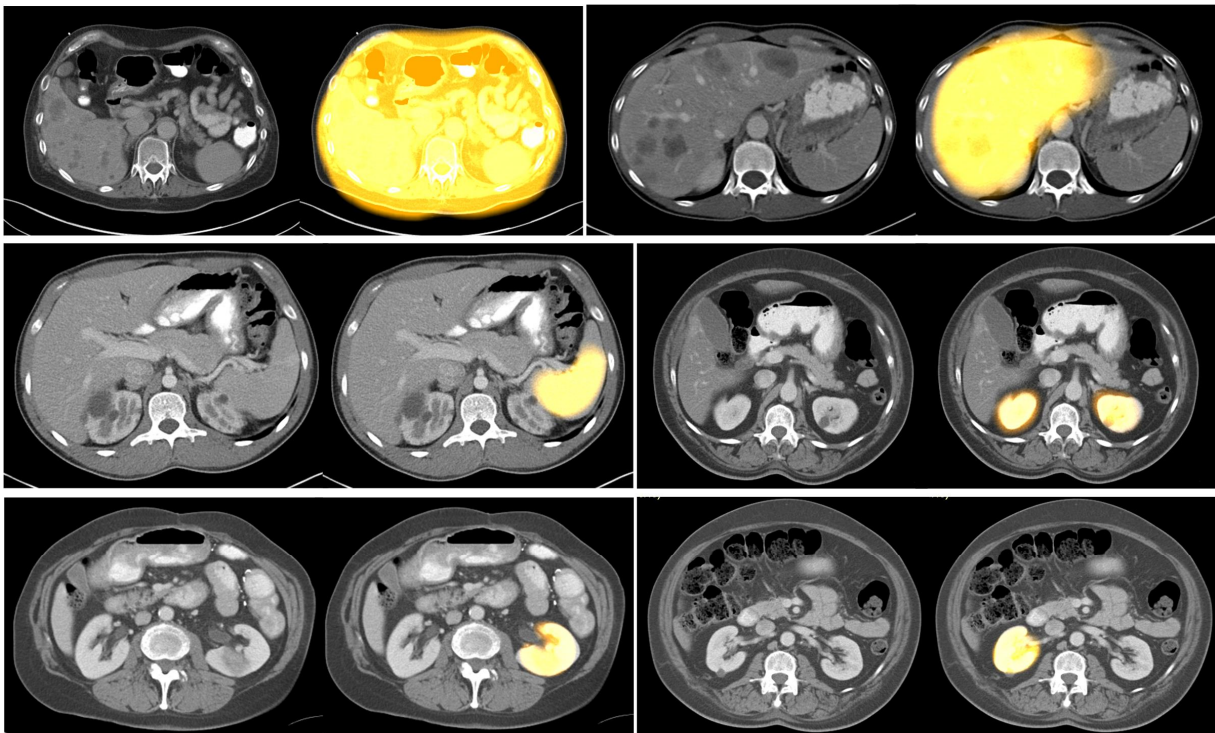


Figure 2. Sample recognition results for the new AAR approach on images from image data set DS2. The models are shown overlaid on the test image slices. The results shown are for the following objects. Top: ASkn, Lvr. Middle: Spl, Kd. Bottom: LKd, Rkd.

Table 1. Location and size error (mean and standard deviation) over the images in DS2 for the new AAR approach.

		ASkn	Lvr	Spln	Kd	Lkd	Rkd
Location error	Mean (mm)	3.02	9.68	9.16	12.9	13.2	14.8
	Standard deviation (mm)	1.29	6.25	8.44	10.2	12.1	13.9
Size error	Mean	1.0	1.0	1.1	1.0	1.0	1.0
	Standard deviation	0.0	0.1	0.1	0.2	0.2	0.2

The modified strategy also improves recognition accuracy on normal images over the original AAR approach in [1]. Table 2 lists location and size errors for images in DS1 when 25 data sets were used for building the models and the remaining data were used for testing. The original results are indicated in parenthesis.

Table 2. Location and size error (mean and standard deviation) over the images in DS1 for the new AAR approach and previous AAR approach (in parenthesis).

		ASkn	Lvr	Spln	Kd	Lkd	Rkd
Location error	Mean (mm)	5.83(5.83)	7.52(7.80)	5.48(10.41)	9.19(9.19)	13.2(13.4)	11.9(12.2)
	Standard deviation (mm)	3.42(3.42)	4.63(5.15)	3.19(11.73)	8.1(8.1)	12.0(12.0)	10.4(10.2)
Size error	Mean	1.0(1.0)	1.0(1.0)	0.9(0.9)	1.0(1.0)	1.0(0.9)	1.0(0.9)
	Standard deviation	0.0(0.0)	0.1(0.1)	0.1(0.1)	0.0(0.0)	0.1(0.0)	0.1(0.0)

4. CONCLUSIONS

(a) Motivated by the goal of direct disease quantification, we present a new AAR strategy which is general and not object-specific and which retains the generality of the spirit of the original AAR approach. Its object localization accuracy is within 1-3 voxels, which is comparable to or better than that of methods in the literature. The new strategy retains the same level of performance or improves on the previous AAR approach on near normal images.

(b) The strategy presented here works for blob-like solid organs without significant concavities. For the latter type of objects, other strategies can be devised to make sure that the sampled regions are properly inside the object of interest in the given image.

REFERENCES

- [1] Udupa, J.K., Odhner, D., Zhao, L.M., Tong, Y.B., Matsumoto, M.M.S., Ciesielski, K.C., Falcao, A.X., Vaideeswaran, P., Ciesielski, V., Saboury, B., Mohammadianrasanani, S., Sin, S., Arens, R., and Torigian, D.A. , "Body-wide hierarchical fuzzy modeling, recognition, and delineation of anatomy in medical images," *Med Image Anal* 18(5), 752-771 (2014)
- [2] Bagci, U., Udupa, J.K., Mendhiratta, N., Foster, B., Xu, Z.Y., Yao, J.H., Chen, X.J., and Mollura, D.J., "Joint segmentation of anatomical and functional images: Applications in quantification of lesions from PET, PET-CT, MRI-PET, and MRI-PET-CT images," *Med Image Anal* 17(8), 929-945 (2013)
- [3] Barbosa, E.M., Song, G., Tustison, N., Kreider, M., Gee, J.C., Geftter, W.B., and Torigian, D.A., "Computational Analysis of Thoracic Multidetector Row HRCT for Segmentation and Quantification of Small Airway Air Trappin Emphysema in Obstructive Pulmonary Disease," *Acad Radiol* 18(10), 1258-1269 (2011)
- [4] Pham, D.L., Xu, C.Y., and Prince, J.L., "Current methods in medical image segmentation," *Annu Rev Biomed Eng* 2, 315-337(2000)
- [5] Heimann, T., and Meinzer, H.P. , "Statistical shape models for 3D medical image segmentation: a review," *Med Image Anal* 13(4), 543-563(2009)
- [6] Ma, Z., Tavares, J.M., Jorge, R.N., and Mascarenhas, T. , "A review of algorithms for medical image segmentation and their applications to the female pelvic cavity," *Comput Methods Biomech Biomed Engin*13(2), 235-246 (2010)
- [7] Lin, D.T., Lei, C.C., and Hung, S.W., "Computer-aided kidney segmentation on abdominal CT images," *Ieee T Inf Technol B* 10(1), 59-65 (2006)
- [8] Sun, S.H., Bauer, C., and Beichel, R. , "Automated 3-D Segmentation of Lungs With Lung Cancer in CT Data Using a Novel Robust Active Shape Model Approach," *Ieee T Med Imaging* 31(2), 449-460 (2012)

- [9] Meng, L., and Zhao, H. ,"A New Lung Segmentation Algorithm for Pathological CT Images," Proc. International Joint Conference on Computational Sciences and Optimization 1, 847-850 (2009)
- [10] Li, Y.a.M., Zhuang and Wang, Bin,"Segmentation of lung CT with pathologies based on adapt active appearance models," Computer Science and Network Technology (ICCSNT), 2013 3rd International Conference on, 1119-1121 (2013)
- [11] Prasad, M.N., Brown, M.S., Ahmad, S., Abtin, F., Allen, J., da Costa, I., Kim, H.J., McNitt-Gray, M.F., and Goldin, J.G. ,"Automatic segmentation of lung parenchyma in the presence of diseases based on curvature of ribs," Acad Radiol15(9), 1173-1180 (2008)
- [12] Wang, J.H., Li, F., and Li, Q. ,"Automated segmentation of lungs with severe interstitial lung disease in CT," Med Phys 36(10), 4592-4599 (2009)
- [13] Sluimer, I., Prokop, M., and van Ginneken, B. ,"Toward automated segmentation of the pathological lung in CT," Ieee T Med Imaging 24(8), 1025-1038 (2005)